

# The role of wave energy accumulation in tropical cyclogenesis over the tropical North Atlantic

James M. Done · Greg J. Holland · Peter J. Webster

Received: 30 June 2009 / Accepted: 6 July 2010 / Published online: 10 August 2010  
© Springer-Verlag 2010

**Abstract** A hierarchical modeling approach is used to study the process by which interactions of easterly waves with the background flow can result in a reduction in the longitudinal and vertical scale of the waves. Theory suggests that in flows that possess a negative longitudinal gradient ( $U_x < 0$ ) there is a reduction of longitudinal and vertical group speeds and an increase in regional wave action density (or “wave energy”). Relative vorticity increases locally leading to an increase in the likelihood of tropical cyclogenesis near the wave axis. Opposite impacts on the structure of the waves is expected in a  $U_x > 0$  domain. In the simplified framework of a free-surface and divergent shallow water model, Rossby wave properties are tracked through a range of background flow scenarios to determine the important scales of interaction. The importance of wave energy accumulation for tropical cyclogenesis is then studied in a full physics and dynamics model using a nested regional climate model simulation, at 12 km horizontal grid spacing, over the tropical North Atlantic region for the entire 2005 hurricane season. The dynamical environment within which 70% of easterly waves formed tropical cyclones exhibits coherent regions in which easterly winds increase towards the east, consistent with the occurrence of wave energy accumulation.

**Keywords** Tropical cyclogenesis · African easterly waves · Shallow water model · Nested regional climate model

## 1 Introduction

Climatological conditions suitable for tropical cyclogenesis have been known for decades (e.g. Gray 1968; Briegel and Frank 1997; Ritchie and Holland 1999). Frank and Roundy (2006) distil these conditions into four general characteristics: warm sea surface temperatures coupled with a deep oceanic mixed layer; cyclonic low-level relative vorticity and planetary vorticity; weak to moderate vertical wind shear; and high mid-level relative humidity. These conditions are frequently met during the hurricane season, yet the multitude of cloud clusters that do not develop into tropical cyclones suggests such broad climatological conditions are not sufficient.

The climate of the low latitudes is characterized by a high level of wave activity, as shown for example in Wheeler and Kiladis (1999). Frank and Roundy (2006) suggest these transient modes act to provide a local enhancement of regions already favorable for cyclogenesis by increasing ambient relative vorticity, enhancing ascent and humidity, modifying vertical shear or any combination of all three. Indeed, many studies have identified the importance of wave activity for tropical cyclone formation (e.g. Ritchie and Holland 1999; Thorncroft and Hodges 2001; Frank and Roundy 2006; Molinari et al. 2007).

The summer climate of the tropical North Atlantic is dominated by easterly waves in the lower troposphere (Thorncroft and Hodges 2001). These waves are generated and maintained due to strong diabatic heating aloft in the ITCZ and shear instability of the African easterly jet

---

J. M. Done (✉) · G. J. Holland  
National Center for Atmospheric Research,  
P.O. Box 3000, Boulder, CO 80307, USA  
e-mail: done@ucar.edu

P. J. Webster  
Georgia Institute of Technology, Atlanta GA, USA

(e.g. Hsieh and Cook 2005) and are known to be associated with at least half of all Atlantic tropical cyclones (Frank and Clark 1980; Pasch et al. 1998) and almost all category 4 and 5 Atlantic hurricanes (Landsea 1993). However, there is less agreement on the specific mechanisms that produce a tight vortex from a larger scale wave and on their relative contributions to cyclogenesis.

Waves in the tropics propagate through a background state of substantial variability in latitude, longitude and with height. Farrell and Watterson (1985) described in theoretical terms a mechanism for wave modification through interaction with the background flow. This linear theory is based on the notion of scale separation such that the change in the background flow over the scale of the wave is small, and states that a Rossby wave propagating through a region of flow becoming more positive may reach a stopping point where the background flow is equal and opposite to the group velocity and may result in a reflection of the wave. However, these calculations were conducted under the constraints of a barotropic atmosphere. When a baroclinic fluid is considered, a much richer behavior of waves in a variable basic state is found. Using the ray-tracing technique of Lighthill (1978), Webster and Chang (1988) were able to show for a Rossby wave where the frequency of the wave is conserved that wave number ( $k$ ) along the wave trajectory is determined by the kinematic relation:

$$\frac{dk}{dt} = -k \frac{\partial U}{\partial x} \quad (1)$$

which states that the wave will expand or shrink in longitudinal scale depending on the sign of the longitudinal ( $x$ ) gradient in the background flow ( $U$ ). Thus, zonal flow becoming more westerly in the direction of propagation has two simultaneous effects on a Rossby wave: a simple Doppler shift of group and phase velocities, and a decreasing wavelength and associated decreasing group and phase velocity. We thus refer to areas where  $U_x < 0$  as wave accumulation regions. Using Eq. 1 we can calculate the change in longitudinal wave number  $k$  as a function of time moving through a constant stretching deformation field, as shown in Fig. 1a. The constant stretching deformation field used here,  $dU/dx \approx -0.8 \times 10^{-6} \text{ s}^{-1}$ , is representative of a typical summer season average value found over the tropical North Atlantic and was determined by an examination of NCEP-NCAR reanalysis data (not shown).

The decreasing group speed attending increases in  $k$  has another important effect. Whitham (1965) and Bretherton and Garrett (1968) found that the wave action density,  $\xi = E/\omega_r$  where  $E$  is the energy density of the wave and  $\omega_r$  is the frequency in a local frame of reference, is conserved along a ray, i.e.,

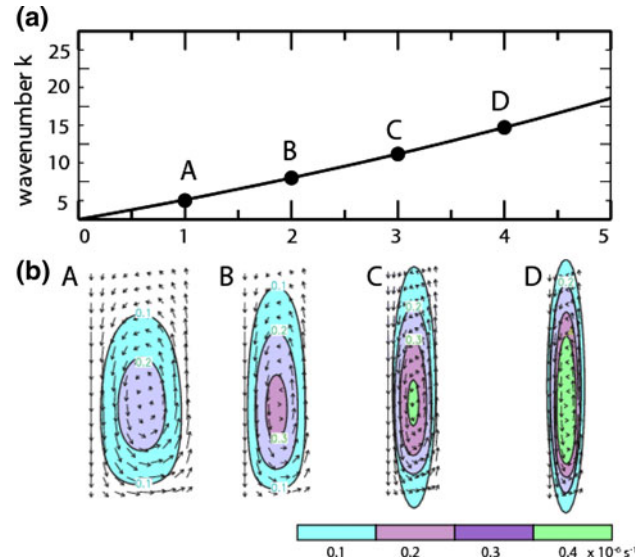


**Fig. 1** **a** Change in longitudinal wave number  $k$  as a function of time over a 5-day period moving through a constant stretching deformation field ( $du/dx \approx -0.8 \times 10^{-6} \text{ s}^{-1}$ ). **b** Change in the longitudinal structure of the low pressure part of the wave showing wind vectors and relative vorticity (colors,  $\text{s}^{-1}$ ). Letters correspond to the times marked in **a**

$$\frac{\partial \xi}{\partial t} + \frac{\partial (C_{\text{gd}} \xi)}{\partial x} = 0 \text{ or } \frac{\partial \xi}{\partial t} + C_{\text{gd}} \frac{\partial \xi}{\partial x} = -\xi \frac{\partial C_{\text{gd}}}{\partial x} \quad (2)$$

where  $C_{\text{gd}}$  is the local Doppler shifted longitudinal group speed. For equatorially trapped Rossby and Kelvin waves,  $\omega_r$  and  $C_g$  do not depend explicitly on  $x$  and  $t$  for a slowly varying background state. Webster and Chang (1988) used expressions for the local Doppler shifted group speed (not shown) in Eq. 2 to show that for a slowly varying background state the energy density of the wave  $E (= \rho g h^2 / 2$  where  $\rho$  is the density of the fluid and  $h$  is the surface perturbation height) changes as:

$$\frac{\partial E}{\partial t} + C_{\text{gd}} \frac{\partial E}{\partial x} = -E \frac{\partial U}{\partial x} \quad (3)$$

Therefore, as  $C_{\text{gd}} \rightarrow 0$  in regions of wave accumulation,  $E$  will increase. Furthermore, relative to these changes, the cyclonic relative vorticity will also increase enhancing the local cyclonic vorticity in the wave trough. We do not have analytic solutions for relative vorticity; however, using wave solutions to the shallow water equations on an equatorial  $\beta$ -plane, as described in “Appendix”, and if we know the change of  $k$  in a stretching deformation field, as shown in Fig. 1a, then we can also calculate the change in relative vorticity. During its propagation towards the west, the wave reduces its longitudinal scale, increases its energy density and increases its relative vorticity as shown in Fig. 1b.

Webster and Chang (1997) showed variations in the background flow can also modify waves meridionally and

vertically and is certainly possible for a wide range of modes. Again following Lighthill (1978) and Webster and Chang (1988, 1997) the vertical wave number ( $m$ ) changes as:

$$\frac{dm}{dt} = -k \frac{\partial U}{\partial z} \quad (4)$$

Thus, westerly shear enhances vertical propagation of a Rossby wave while easterly shear inhibits vertical propagation. Easterly shears thus results in a vertical trapping of wave energy in the lower troposphere.

Despite the expectation of a breakdown of linear theory in the region of accumulation, where the characteristic scale of the background flow varies considerably, linear theory has been shown in many problems to give qualitatively correct results. Chang and Webster (1990), for example, show that accumulation possesses much the same character in the linear and nonlinear regime due to the dominance of convergence of advection by the background flow. Kuo et al. (2001) also find that in linear theory, accumulation occurs primarily by convergence of zonal advection by the background flow, but in the absence of other forcing (i.e. diabatic effects) wave energy will eventually be lost due to Reynold's stress. In the non-linear regime, however, contraction of zonal wave scale plays the critical role in maintaining wave energy accumulation.

Thus, easterly waves propagating through a wave accumulation zone in the presence of easterly shear with height will shrink, slow down, become more energetic (through a concentration of energy) in the lower levels, and exhibit increased cyclonic vorticity in the wave trough. All of these processes enhance the potential for tropical cyclone development. Holland (1995) proposed wave accumulation as a contributing mechanism for cyclone development over the tropical Western Pacific. Using ray tracing techniques on reanalysis data, Sobel and Bretherton (1999) argued that wave accumulation is important for the growth of low-level synoptic disturbances in this region, and can dominate local diabatic effects. Using a non-divergent barotropic vorticity model, Kuo et al. (2001) show that large-scale convergence, wave scale contraction, and nonlinear dynamics on the beta plane all contribute to the initial development of a vortex in a confluence zone representative of flow over the West Pacific and, importantly, show that diabatic processes are not necessary for vortex formation. More recently, Tam and Li (2006) also showed wave accumulation to be important for the growth of low-level synoptic disturbances in this region in reanalysis data. These studies show accumulation due to contraction of the zonal wave scale to be as strong, and sometimes much stronger, than that due to mere convergence of the mean flow.

Webster and Chang (1997) note that analytic theory and results from simple numerical models may not transfer easily to full physics and dynamics atmospheric models within which waves contend with variable temperature and moisture and diabatic processes. In addition, the notion of scale separation and background flow becomes ill-defined. However, there is promise that the simple results will be correct at least qualitatively, as evidenced by the success of Li et al. (2003) in simulating accumulation of easterly wave energy and subsequent cyclogenesis under idealized conditions in a full physics, full dynamics hurricane model.

Whether wave energy accumulation plays an important role in tropical cyclogenesis over the tropical North Atlantic is an open question since previous studies have largely focused on the Western Pacific region. Some recent studies, however, have noted the modulation of tropical cyclones over the North Atlantic by low-level flow anomalies attributed to the Madden-Julian Oscillation (MJO) (e.g. Barrett and Leslie 2009). Maloney and Hartmann (2000) show tropical cyclogenesis frequency in the Gulf of Mexico and the western Caribbean is strongly modulated by MJO wind anomalies. They show that westerly phases of the MJO are characterized by low-level westerly wind anomalies ( $U_x < 0$  with enhanced wave energy accumulation) and cyclonic vorticity that extend into the Gulf of Mexico (their Fig. 2a) which also results in a marked increase in tropical cyclone activity. The role of wave energy accumulation in cyclogenesis is of practical relevance since relating wave activity to cyclogenesis has the potential to extend genesis prediction lead times considerably.

Here we adopt a hierarchical modeling approach to assess the importance of wave energy accumulation for cyclogenesis over the tropical North Atlantic. We start in the simplified framework of a free-surface and divergent shallow water model to explore the important scales of wave energy accumulation, both within and outside the validity of scale separation, for flow scenarios representative of the summer climate of the tropical North Atlantic. To identify the importance of the wave accumulation process for tropical cyclogenesis in a full physics and

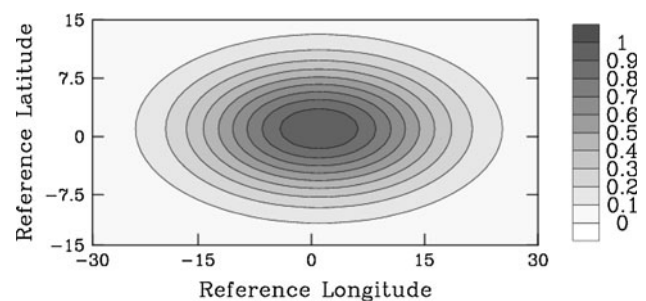


Fig. 2 Spatial functional form of the forcing function. Eq. 9

dynamics model, we examine a simulation conducted using a horizontal grid spacing of 12 km over the tropical North Atlantic region for the entire 2005 hurricane season using the NCAR nested regional climate model (NRCM). The paper is divided into two general areas. Sections 2 and 3 comprise the method and results from the shallow water model experiments. Sections 4 and 5 investigate the importance of wave energy accumulation for tropical cyclogenesis in a full dynamics and full physics regional climate simulation, and examine the applicability of the simple model results. A summary of results is presented in Sect. 6 with discussion of implications for genesis prediction.

## 2 Shallow water model configuration

The framework of the shallow water equations enables exploration of the process of wave accumulation in a horizontal flow that is independent of height, and, importantly, in the absence of the effects of temperature and moisture fields and associated diabatic effects. The experimental design follows closely that of Webster and Chang (1988) in which Rossby waves are generated and propagate through a range of background states. Their model set-up was representative of the equatorial upper-troposphere and focused on connections to the extratropics. Here we create conditions representative of low-levels over the tropical North Atlantic in the absence of shear; that is, off-equatorial Rossby waves propagating through a zonally varying background zonal flow. Properties of Rossby waves are tracked through different background states to examine wave modification through wave accumulation.

### 2.1 Model description

The shallow water model is taken from the Flexible Modeling System suite of models developed at the Geophysical Fluid Dynamics Laboratory. The equations describe hydrostatic incompressible flow on the surface of a rotating sphere in spherical co-ordinates. The momentum and continuity equations complete the equation set and the inviscid and unforced equations can be written in terms of the zonal and meridional wind ( $u$  and  $v$ ) and the geopotential,  $\Phi$ , as:

$$\frac{\partial u}{\partial t} = fv - \frac{u}{a \cos(\theta)} \frac{\partial u}{\partial \lambda} - \frac{v}{a} \frac{\partial u}{\partial \theta} + \frac{uv \tan(\theta)}{a} - \frac{1}{a \cos(\theta)} \frac{\partial \Phi}{\partial \lambda} \quad (5)$$

$$\frac{\partial v}{\partial t} = -fu - \frac{u}{a \cos(\theta)} \frac{\partial v}{\partial \lambda} - \frac{v}{a} \frac{\partial v}{\partial \theta} + \frac{u^2 \tan(\theta)}{a} - \frac{1}{a} \frac{\partial \Phi}{\partial \theta} \quad (6)$$

$$\frac{D\Phi}{Dt} = -\Phi \nabla \cdot \underline{v} \quad (7)$$

where  $\theta$  is latitude,  $\lambda$  is longitude,  $a$  is a constant Earth radius,  $f$  is the coriolis parameter, and  $\underline{v}$  is the total flow. The choice of the background geopotential,  $\Phi_0$ , determines the degree to which the modes are divergent. If  $\Phi_0$  is very large (deep fluid) then the modes are essentially non-divergent. As  $\Phi_0$  decreases the modes become increasingly divergent.

The model has one layer of fluid with a free upper surface and a flat, rigid lower boundary, and can be interpreted as a shallow layer of fluid in the lower troposphere. However, the formulation represents the first baroclinic mode of a baroclinic atmosphere and is thus representative to some extent of the deep tropics (Webster 1972; Gill 1980). The resolution is set at T85 which corresponds to a grid spacing of approximately 150 km and is sufficient to resolve synoptic scale variability. This model describes wave propagation through a variable background flow without the need for scale separation requirements and is fully nonlinear enabling an examination of the full interaction between waves and the background state.

### 2.2 Generation of the background states

Environmental low-level flow conditions representative of the tropical North Atlantic are created using a carefully constructed forcing. This forcing spins up a large-scale off-equatorial circulation resulting in variable zonal flow at low latitudes. The integration starts from a state of rest, in the rotating frame, with uniform  $\Phi$ . Flow is generated by relaxing  $\Phi$  to a field of geopotential that varies with latitude and longitude,  $\Phi_{\text{eq}}(\theta, \lambda)$ , over a timescale set to 10 days. We set:

$$\Phi_{\text{eq}} = \Phi_0 + \frac{A}{\sqrt{2\pi}} e^{\left( \frac{-(\lambda-\lambda_0)^2}{2\sigma_\lambda^2} - \frac{(\theta-\theta_0)^2}{2\sigma_\theta^2} \right)} \quad (8)$$

where  $\Phi_0$  represents the base state equivalent depth,  $A$  is the amplitude and  $\sigma_\theta$  and  $\sigma_\lambda$  are the spatial scales in latitude and longitude respectively. The function follows a normal decay away from an arbitrary central latitude and longitude  $(\theta_0, \lambda_0)$ , set here to be (17°N, 55°W) to generate a flow anomaly across the longitudes of the tropical North Atlantic. For all experiments we set the base state equivalent depth,  $\Phi_0$ , equal to  $800 \text{ m}^2 \text{ s}^{-2}$  to be inside the meteorologically significant range of waves confined to the troposphere (e.g. Webster and Chang 1988; Wheeler et al. 2000) and to generate Rossby waves of phase speeds representative of African easterly waves; that is,  $6\text{--}8 \text{ m s}^{-1}$  (Reed et al. 1988). The value of  $\Phi_0$  (equivalent to a fluid of roughly 80 m) also ensures that the modes are divergent.

The velocities are relaxed linearly to zero over a timescale set to 20 days. The model achieves a steady state after 75 days of integration after which the relaxation and steady background state are maintained throughout the experiments.

### 2.3 Generation of Rossby waves

Once the model has achieved steady state, an imposed transient forcing generates an off-equatorial Rossby wave that has similar properties to a typical African easterly wave. This transient forcing follows the functional form used in Webster and Chang (1988) and has normal decay in space from a central latitude and longitude  $(\theta_{f0}, \lambda_{f0})$  as:

$$\Phi_f(\theta, \lambda) = A_f e^{-\left(\frac{(\theta-\theta_{f0})^2}{l_\theta^2} + \frac{(\lambda-\lambda_{f0})^2}{4l_\lambda^2}\right)} \tag{9}$$

where  $A_f$  is the amplitude and  $l_\theta$  and  $l_\lambda$  are the spatial scales in latitude and longitude respectively. This spatial functional form is shown in Fig. 2. The choice for the central latitude and longitude  $(\theta_{f0}, \lambda_{f0})$  is arbitrary but for reference set to  $(0^\circ\text{N}, 5^\circ\text{W})$  to represent the location of a typical heating anomaly associated with deep convection over the African continent. Following Webster and Chang (1988), and shown in Fig. 3, the temporal variation of the forcing function follows:

$$\Phi_f(t) = \left(\frac{t^3}{2\delta^3}\right) e^{-\left(\frac{t}{\delta}\right)} \tag{10}$$

where the decay timescale,  $\delta$ , is set to 6 h.

### 2.4 Experiments

Three background states are generated. A background state with zero flow everywhere is used as a reference experiment against which to compare experiments using two non-

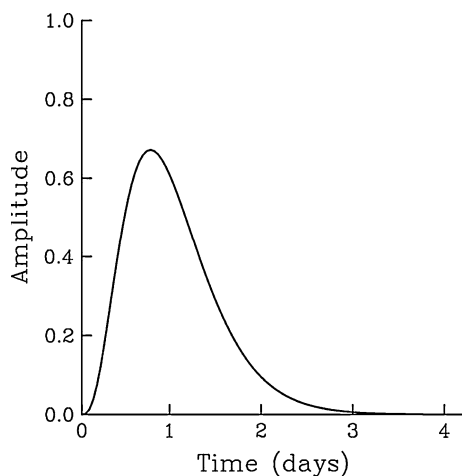


Fig. 3 Temporal functional form of the forcing function. Eq. 10

zero flow background states; one with a negative gradient of zonal flow ( $U_x < 0$ ) and the other with a positive gradient of the zonal flow ( $U_x > 0$ ). Hereafter, these background states are referred to as scenarios U0, UN and UP respectively and act as initial conditions for the numerical experiments.

The amplitude  $A$  in Eq. 8 is set to  $2,000 \text{ m}^2 \text{ s}^{-2}$  and the spatial scales,  $l_\theta$  and  $l_\lambda$  are set to  $8^\circ$  and  $22.5^\circ$  which together control the magnitude of the background height, and therefore also flow anomalies. Using NCEP-NCAR reanalysis data the observed range of  $U_x$  between  $60^\circ\text{W}$  and  $20^\circ\text{W}$  and averaged over  $10^\circ\text{N}$ – $20^\circ\text{N}$  for August–September–October average for the years 1948–2007 is  $-1.8 \times 10^{-6} \text{ s}^{-1}$  to  $+0.2 \times 10^{-6} \text{ s}^{-1}$  with an average value of  $-0.8 \times 10^{-6} \text{ s}^{-1}$ . The values of  $U_x$  in experiment UN are carefully constructed not to exceed this observed range with a typical value close to the observed average of  $-0.8 \times 10^{-6} \text{ s}^{-1}$ . The equations for the generation of UN and UP are identical except for a reversal of sign in Eq. 8. The background flow fields for UN and UP are shown in Fig. 4. These fully non-linear background flows contain both zonal and meridional stretching and shearing deformation fields, but we focus our analysis only on variations following the trajectory of the Rossby wave which is largely zonal and has only a negligible meridional component.

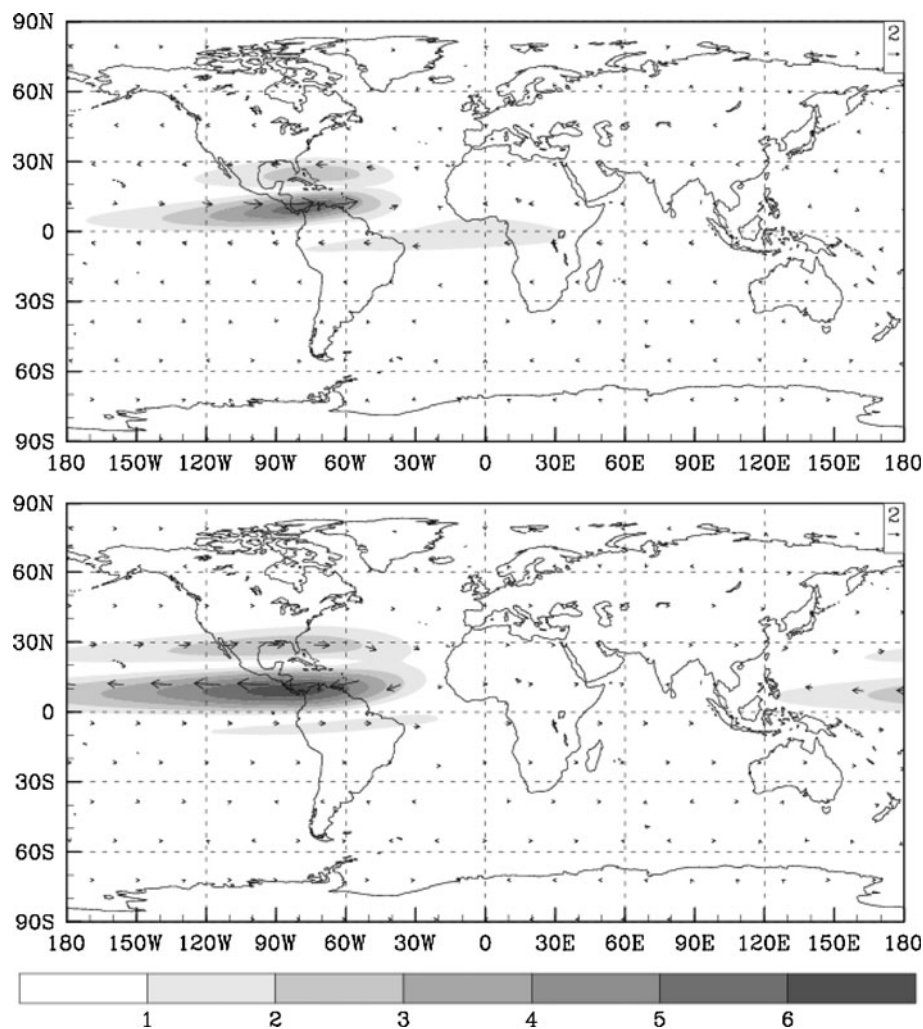
We first construct scenarios in which scale separation is satisfied; that is, the zonal scale of the background flow anomaly is large compared to the zonal scale of the Rossby wave. Scales  $l_\theta$  and  $l_\lambda$  in Eq. 9 are set to  $8^\circ$ , which corresponds to an initial zonal wave scale of approximately 4,000 km. These set of 3 experiments are known as set SS hereafter. We then repeat the experiments but change the zonal scale of the Rossby wave to be equal to the zonal scale of the background flow anomaly; that is,  $22.5^\circ$ , such that scale separation is not satisfied. These set of 3 experiments are known as set NSS hereafter. All experiments run for 25 days.

## 3 Shallow water model results

We track properties of Rossby waves through the three different background flow scenarios described in the previous section. Specifically, we track zonal wave scale, phase speed and maximum relative vorticity.

First we consider the case for which scale separation is satisfied (experiment set SS). Figure 5 shows Hovmöller diagrams of perturbation geopotential at  $11^\circ\text{N}$  for three experiments corresponding to scenarios U0, UN and UP together with a cross section of the background zonal flow at the same latitude. For U0, the forced perturbation grows and decays over approximately 2 days followed by a wave

**Fig. 4** The background flow ( $\text{m s}^{-1}$ ) for scenario UN (*top*) and scenario UP (*bottom*) used as initial conditions for the shallow water experiments. The continental outlines are indicative only and there is no land differentiation in the shallow water model



response in the form of a fast eastward propagating equatorial Kelvin wave and a slower westward propagating off-equatorial Rossby wave. Signatures of interference with faster equatorial inertia-gravity waves can also be seen along the Rossby wave trajectory. Rossby wave dispersion can also be seen with the longer wavelengths in the packet having faster phase speeds. For UN, the Rossby wave maintains higher amplitude, in terms of perturbation geopotential, than for U0 and also a suggestion of a contracting zonal wave scale and a decreasing phase speed. The opposite is true for scenario UP for which the Rossby wave loses amplitude compared to the UN and U0 and experiences an expanding zonal wave scale and increasing phase speed.

The differences between the three experiments are further illuminated by examining the evolution of wave characteristics. Time series of zonal wave scale, defined here as twice the distance between the westernmost trough and ridge phase lines, for the three experiments is shown in Fig. 6a. For U0, the wave scale increases due to Rossby wave dispersion. The relative impact of a zonally varying

background state is scale contraction for UN and scale expansion for UP. The time series of phase speed, calculated by tracking the trough phase line in time and shown by the thick solid and dashed lines in Fig. 6b, the impact of a zonally varying background state is a slowing down for UN and a speeding up for UP, consistent with the changing in wave scale. These changes are of much larger magnitude than the slight increase in phase speed for U0 due to wave dispersion and is an indication of the importance of wave accumulation processes. In Fig. 6b the flow relative phase speed variation arises entirely from changes in wave scale, whereas ground relative phase speed variations respond to both divergence of advection and changes in wave scale. These indicate that the wave accumulation due to scale contraction is as important as that due to divergence of the flow.

Time series of maximum relative vorticity associated with the Rossby wave (Fig. 6c) show the relative impact of a zonally varying flow against a general decreasing trend for U0 is to decrease relative vorticity for UP but substantially increase relative vorticity for UN. At day UN 10

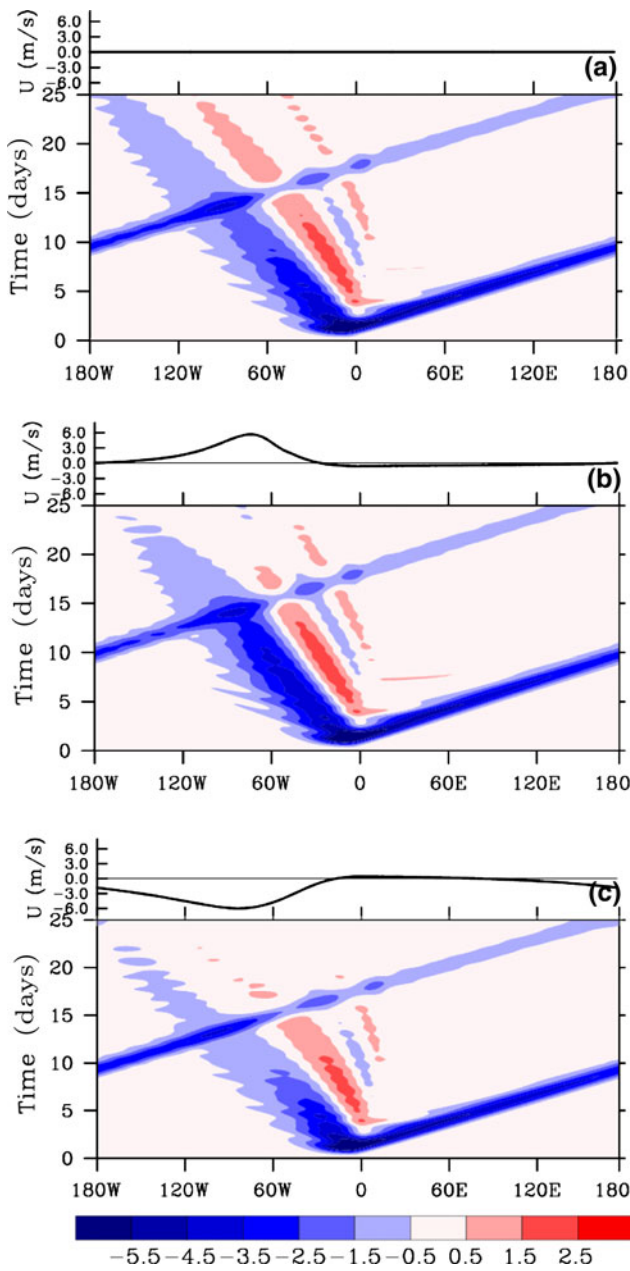


**Fig. 5** Time-longitude diagrams of perturbation geopotential (shaded,  $m^2 s^{-2}$ ) at  $11^\circ N$  for three experiments corresponding to scenarios **a** U0, **b** UN and **c** UP for experiment set SS. Also shown for reference above each panel is a cross section of the background zonal flow ( $m s^{-1}$ ) at  $11^\circ N$  at initial time

relative vorticity has amplified to 3.5 times that in U0. The sign of the relative changes in wave scale and phase speed are all consistent with the linear theory of wave accumulation.

The case for which scale separation is violated is now examined (experiment set NSS, for which the zonal scales of the Rossby wave and the background flow anomalies in UN and UP are the same). Hovmöller plots for U0, UN and UP for set NSS in Fig. 7 indicate that the wave response in

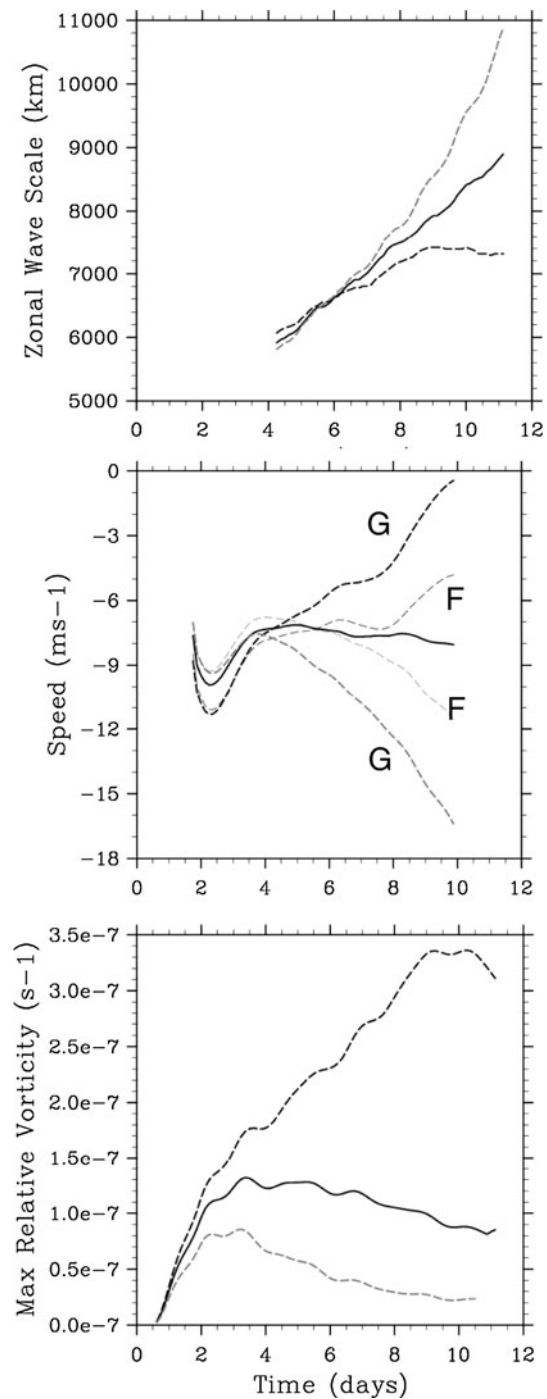


**Fig. 6** Timeseries of Rossby wave properties through scenario U0 (black solid line), UN (black dashed line) and UP (gray dashed line) for experiment set SS. **a** Zonal wave scale (km), **b** ground relative phase speeds (thick lines and marked ‘G’) and flow relative phase speeds (thin lines and marked ‘F’) and **c** maximum relative vorticity ( $s^{-1}$ )

U0 is much the same as in the previous set of experiments, as expected. The relative changes in zonal wave scale, phase speed and amplitude between U0, UN and UP are qualitatively similar to experiment set SS (Fig. 5).

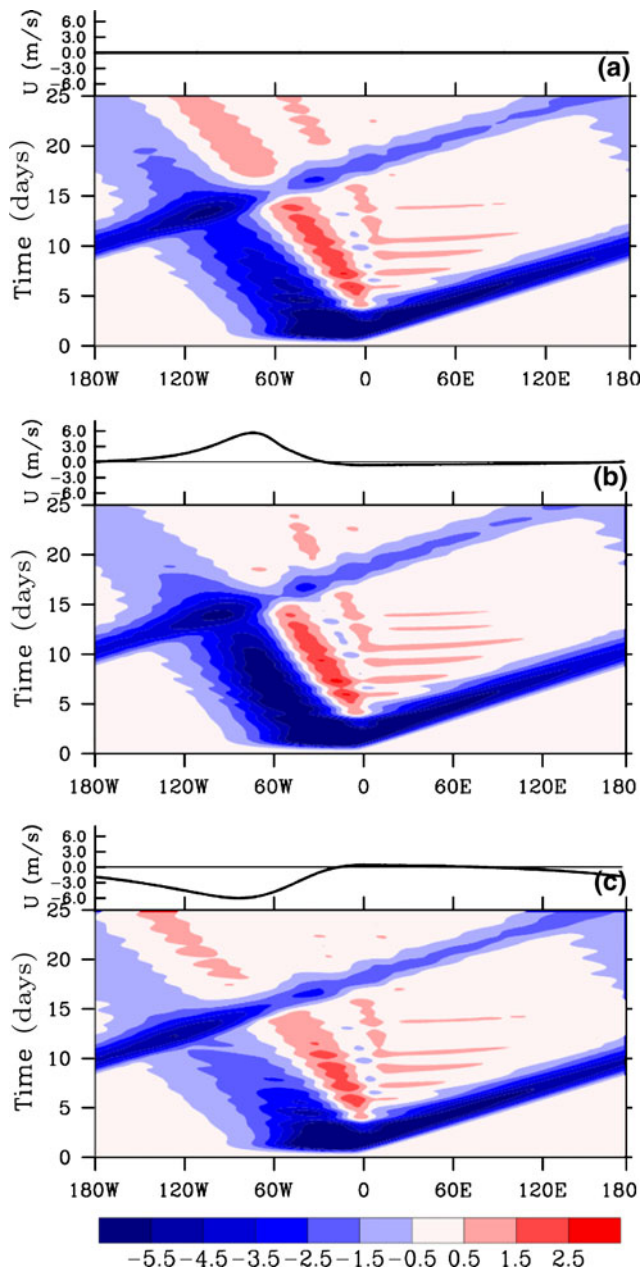


Fig. 7 As in Fig. 5, but for experiment set NSS

The evolution of wave characteristics in Fig. 8 also indicates qualitative similarity between experiments SS and NSS. The phase speeds following the wave trajectory are larger for NSS than for SS, due to the longer wavelengths that were imposed. The change in zonal wave scale (and therefore also the change in phase speed) and maximum relative vorticity are also greater for NSS than SS, as expected from Eqs. 1 and 2. Indeed, the maximum relative vorticity for scenario UP is almost 6 times that in scenario U0 for set NSS compared to only about 3.5 times for set SS.

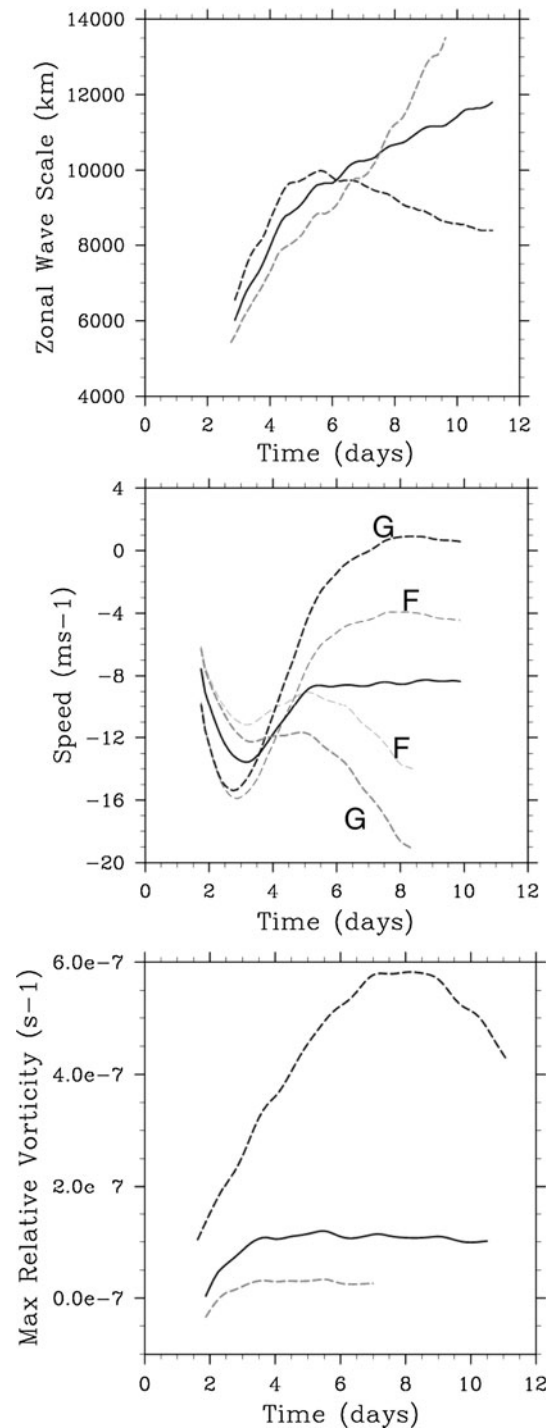


Fig. 8 As in Fig. 6, but for experiment set NSS

The greater growth of relative vorticity during the wave accumulation process for longer wavelengths implies that larger African easterly waves may be more conducive to cyclone formation than smaller ones. We are unaware of any observational studies that have considered wave size and suggest that this provides an observational test of the modeling results.



#### 4 Nested regional climate model set-up

Simulations of tropical climate using multiple levels of nesting of the National Center for Atmospheric Research NRCM were performed primarily to address the multi-scale interactions between deep tropical convection and the tropical climate. These rich datasets are exploited here to examine specifically wave accumulation and tropical cyclogenesis over the tropical North Atlantic region.

##### 4.1 Model setup

The NRCM is based on the Advanced Research Weather Research and Forecasting (WRF) model (Skamarock et al. 2005) version 2.1.1. The WRF model is well suited to simulating the full dynamics and physics of tropical cyclone lifecycles including genesis (e.g. Kieu and Zhang 2008) and major structural characteristics including eye wall and spiral rain bands and the range of observed intensities (Davis et al. 2008). The model has been shown capable of long-term integrations (e.g. Done et al. 2006) with the addition of some minor code modifications; a wide boundary relaxation zone, and an updated lower boundary condition, as described later in this section. A hydrostatic pressure vertical co-ordinate is used with 50 levels such that levels are terrain following near the surface transitioning to pressure surfaces near the model top at 10 mb. Resolution is highest in the boundary layer to capture small-scale variability.

Shortwave and longwave radiation is treated using the CAM3 radiation scheme, and includes the radiative effects of ozone and aerosol. Cumulus convection is parameterized using the Eta Kain-Fritsch scheme, including a parameterization of shallow convection. Explicit precipitation processes are parameterized by the WRF single moment 6-class microphysics. Boundary layer and surface processes are represented by the non-local YSU boundary layer scheme, and the Noah land surface model with 5 soil layers, including seasonally varying vegetation fraction based on climatology.

The NRCM is configured as a channel model and covers 45°S to 45°N, using a horizontal grid spacing of 36 km. The channel model is run for 10 years from 1 January 1996 to 1 January 2006. The simulation is initialized only once at the start of the simulation based on large-scale conditions from NCEP/NCAR global reanalysis data at 2.5° lat/lon grid spacing and thereafter driven at the northern and southern lateral boundaries by the six-hourly this reanalysis dataset and at the lower boundary by monthly AMIP SST data at 0.5° lat/lon grid spacing interpolated to six-hourly. Newtonian relaxation is applied over 15 grid points, following Giorgi et al. (1993), and the relaxation coefficients follow a linear-exponential form, following Liang et al.

(2001). A periodic boundary condition is applied at the east–west boundaries, thus converting the typical limited area domain to a channel to allow free propagation of tropical modes.

Within the parent channel domain are multiple nesting configurations, and for this study we concentrate on a nested domain using 12 km grid spacing of  $757 \times 373$  grid points covering the region of the tropical North Atlantic (see Fig. 1 in Holland et al. 2010). This domain is driven at the lateral boundaries by the parent channel domain for the period 1 May 2005 through 1 December 2005 to span most of the 2005 North Atlantic hurricane season. Two-way nesting is used to enable information to pass to and from the more coarse resolution parent channel domain and the higher resolution limited area nest; thereby resulting in a full multi-scale interaction. SST data for this nested domain are derived from weekly AMIP data at 0.5° interpolated to six-hourly.

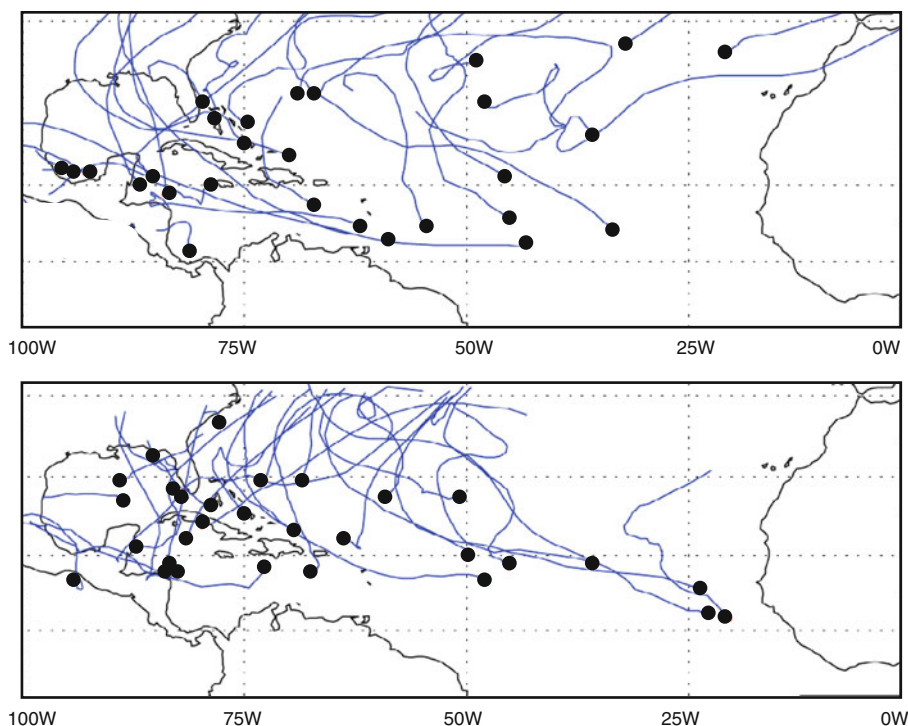
The phase speeds and 3D structure of easterly waves are qualitatively well captured by the NRCM (Tulich et al. 2009). However, the easterly wave filtered rainfall variance is shown to be too low over the North Atlantic but this may be due to a dry bias associated with the model waves. Tulich et al. (2009) also showed good agreement between composites of simulated versus observed cyclogenesis objectively linked to easterly waves. Although Tulich et al. (2009) showed an underestimation in the number of cyclogenesis events between 0 and 15°N for the 36 km parent domain, we show in the next section that the 12 km nested domain produces a more reasonable simulation of low latitude developments. The NRCM simulations therefore provide a suitable dataset to explore the importance of wave accumulation for cyclogenesis in this region.

#### 5 NRCM results

Tropical cyclones in the NRCM are detected and tracked using an automated tracking algorithm. A cyclone is detected using three criteria: (1) the average wind at 1,000 hPa in each of four  $1^\circ \times 10^\circ$  boxes extending North, South, East and West from the center must follow a cyclonic pattern i.e. westward in the North box, southward in West box, etc. in the Northern Hemisphere and opposite in the Southern Hemisphere; (2) the maximum wind speed at 1,000 hPa within  $2^\circ \times 2^\circ$  box surrounding the storm center exceeds  $18 \text{ m s}^{-1}$ ; (3) the 500 hPa temperature has a local maximum within  $2^\circ \times 2^\circ$  box; and the system lasts a minimum of 2 days. The algorithm subsequently tracks the location and characteristics of the cyclone throughout its lifetime.

The full channel model captured the general global and seasonal distributions of tropical cyclones but consistently

**Fig. 9** Initial locations (filled black circles) and tracks (blue lines) of tropical cyclones in the Atlantic Basin during 2005 in (top) the IBTrACS dataset and (bottom) the 12 km nested domain model dataset



overproduced the number of tropical cyclones (not shown). The two-way nested configuration for the 2005 Atlantic hurricane season produced a good simulation of both the number and spatial distribution of tropical cyclones as shown in Fig. 9 with 29 tropical storms compared to 27 in the observations during the period 1 May through 1 December. We focus here on two periods; June through July and August through September. Figure 10 shows cyclogenesis locations and cyclone tracks for these two periods. In total 19 tropical cyclones formed within this 4-month period, 5 in June–July and 14 in August–September. Tropical cyclones that formed in association with an easterly wave were identified using Hovmöller plots of meridional wind at 700 hPa (not shown) to identify signatures of eastward moving disturbances towards genesis time and location. In total 11 tropical cyclones clearly formed in association with an easterly wave; 2 in June–July and 9 in August–September, as indicated in Fig. 10a, b.

Compositing many events eliminates details that vary in time and space between cases and retains features common to all events. Following the approach of Ritchie and Holland (1999) composite fields are obtained by the summation

$$C_{x,y} = \frac{1}{N} \sum_{n=1}^N (A_{x,y})^n \quad (11)$$

where  $(A_{x,y})^n$  is the value at the grid point  $x,y$  of the  $n$ th field, and  $N$  is the number of fields. Composite flow fields for a fixed region  $\pm 20^\circ$  latitude about the composite genesis latitude and  $10^\circ$  West and  $30^\circ$  East of the composite

genesis longitude for the 11 events that formed in association with an easterly wave are shown in Fig. 11. The composite flow fields at genesis time and 3 days before genesis time show the westward propagation of a wave trough towards the composite genesis location and also a second wave trough east of genesis location at genesis time. The apparent wave amplification cannot be fully attributed to the process of wave accumulation since compositing waves of different zonal wavelengths and phase speeds will lead to a decrease in amplitude away from the genesis time and location.

Using Hovmöller plots of meridional wind at 700 hPa and  $20^\circ$ W (not shown), 9 easterly waves were identified in June–July and 13 easterly waves were identified in August–September. The proportion of waves that formed cyclones was 22% in June–July and 69% in August–September. This suggests that some property or combination of properties of either the waves or the environment created more favorable conditions for cyclogenesis in the period August–September. The 2-month mean 700 hPa flow for June–July and August–September (Fig. 12) has some notable differences. The African easterly jet is apparent in both periods but for June–July the jet extends across the entire tropical North Atlantic resulting in an average value of  $U_x$  between  $60^\circ$ W and  $20^\circ$ W averaged over  $10^\circ$ N– $20^\circ$ N of zero with a minimum value of  $-0.3 \times 10^{-6} \text{ s}^{-1}$ . For August–September the jet decreases in magnitude from east to west across the tropical North Atlantic resulting in an average value for  $U_x$  of  $-0.6 \times 10^{-6} \text{ s}^{-1}$  and a minimum of  $-1.0 \times 10^{-6} \text{ s}^{-1}$ .

**Fig. 10** Initial locations (filled circles) and tracks (blue lines) of tropical cyclones that formed in the nested domain in June and July (top) and August and September (bottom). Initial locations of cyclones that formed within an easterly wave are marked in red and those that did not are marked in blue

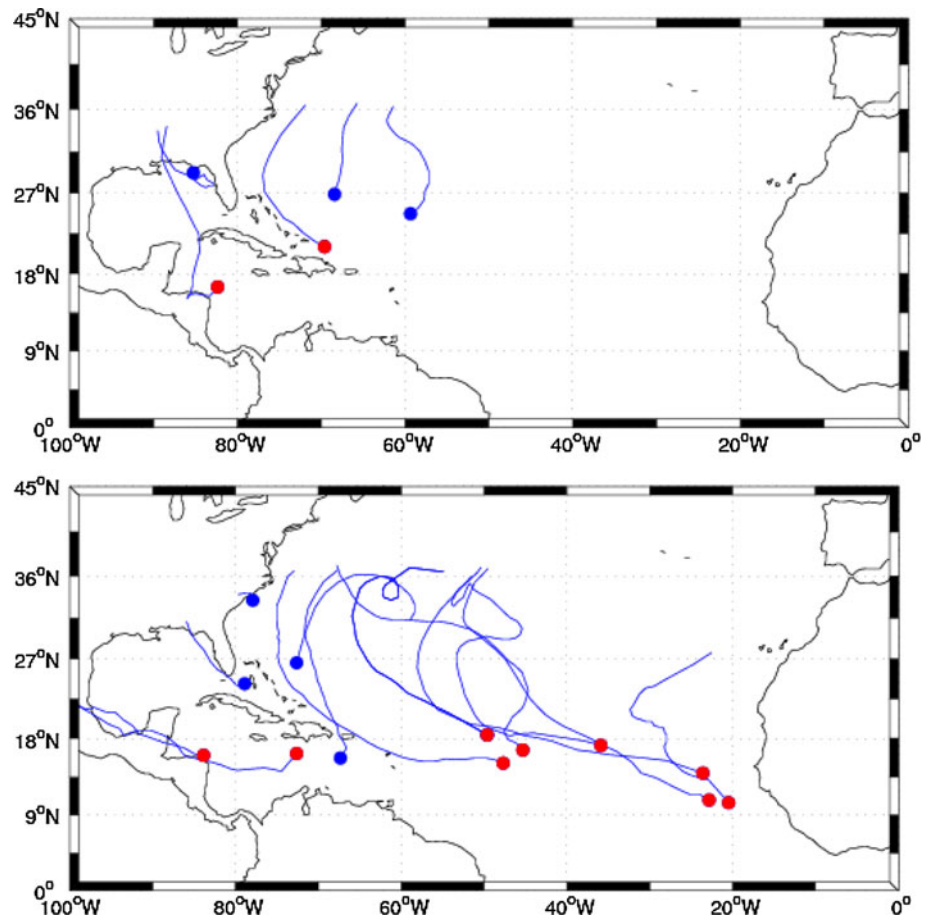
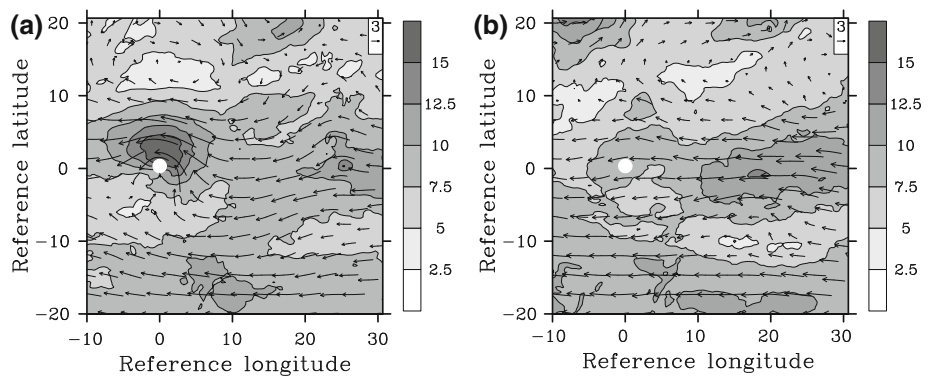


**Fig. 11** Composite wind speed (shaded,  $\text{m s}^{-1}$ ) and wind vectors for a  $40^\circ$  latitude by  $40^\circ$  longitude box surrounding the 11 genesis locations marked by a solid red circles in Fig. 10 at a composite genesis time and **a** 3 days before composite genesis time. The composite genesis location is marked by a solid white circle at reference position ( $0^\circ, 0^\circ$ )

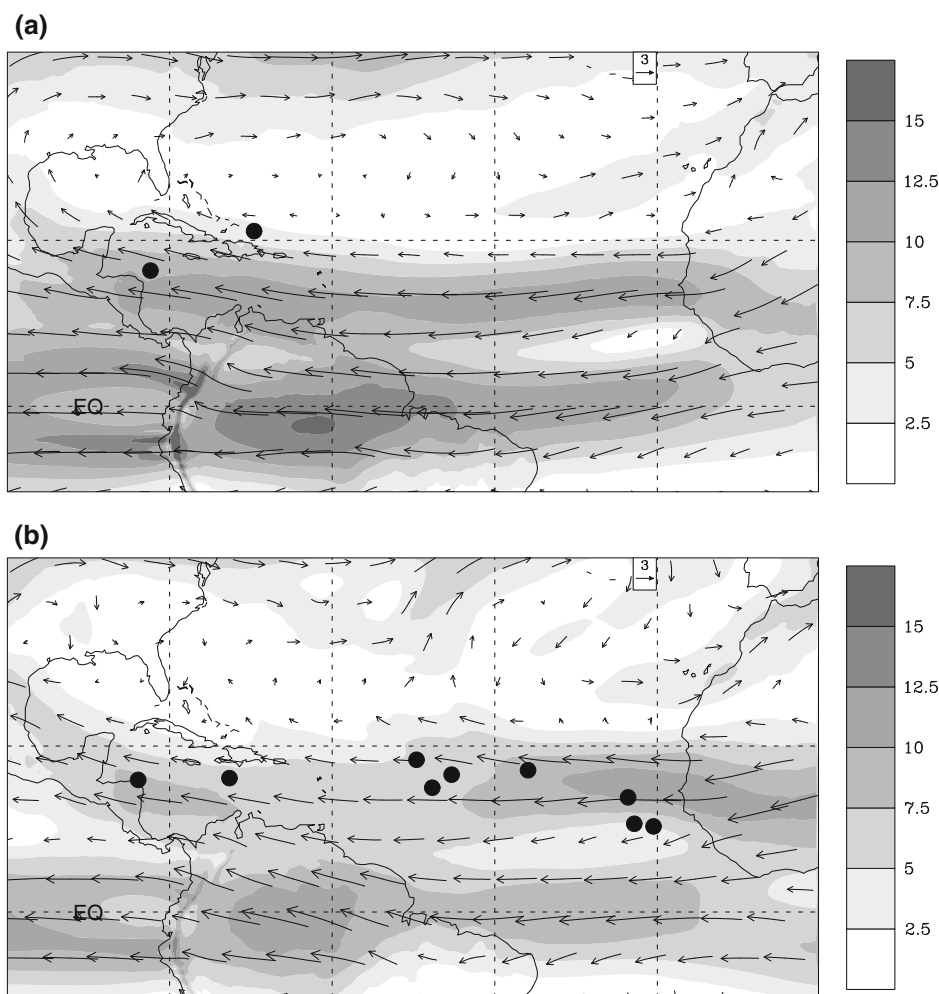


The periods June–July and August–September represent both ends of the observed range of  $U_x$  in the historical record. Assuming the 2-month mean fields are representative of the background flow through which the easterly waves propagate, and that the results of the shallow water experiments in Sect. 3 are qualitatively correct in a full physics and dynamics model, we can hypothesize that in June–July the easterly waves experienced little modification via wave accumulation whereas in August–September

the easterly waves experienced strong modification via wave accumulation that contributed to cyclogenesis.

We note that Swanson (2008) cautioned against using seasonal mean fields as background fields within which cyclones develop due to contamination of the background fields by the cyclones themselves. This is indeed a difficult task, and our experimentation with a variety of other approaches to remove the easterly waves and cyclones and therefore leave a background flow using low pass filtering

**Fig. 12** Wind speed (shaded,  $\text{m s}^{-1}$ ) and wind vectors at 700 hPa for **a** June–July average and **b** August–September average. The 11 genesis locations of cyclones associated with easterly waves are marked by solid black circles



in space and time, wavelet analysis and divergent and rotational analysis, were all unsatisfactory. However, because we focus on regions upstream of the cyclones we consider the mean fields to be representative of the background flow prior to genesis.

Wave accumulation theory states that easterly vertical shear acts to shrink the vertical wave scale (Eq. 4) and trap wave energy in the vertical, leading to an environment more favorable for cyclogenesis. The 2-month mean vertical shear fields, defined here as the difference between the flow at 200 and 850 hPa, for June–July and August–September are shown in Fig. 13. For June–July, strong westerly shear of  $10\text{--}14 \text{ m s}^{-1}$  exists in the region of the African Easterly Jet due to the strong low-level easterlies of the jet beneath upper-level westerlies (not shown). For August–September the strength of the westerly shear in the region of the jet is much weaker, with typical values of  $2\text{--}6 \text{ m s}^{-1}$ . The genesis locations in Fig. 13b are generally in regions of small magnitude shear, as expected due to the inhibiting effect of strong shear on genesis. Owing to genesis within both regions of weak westerly and weak

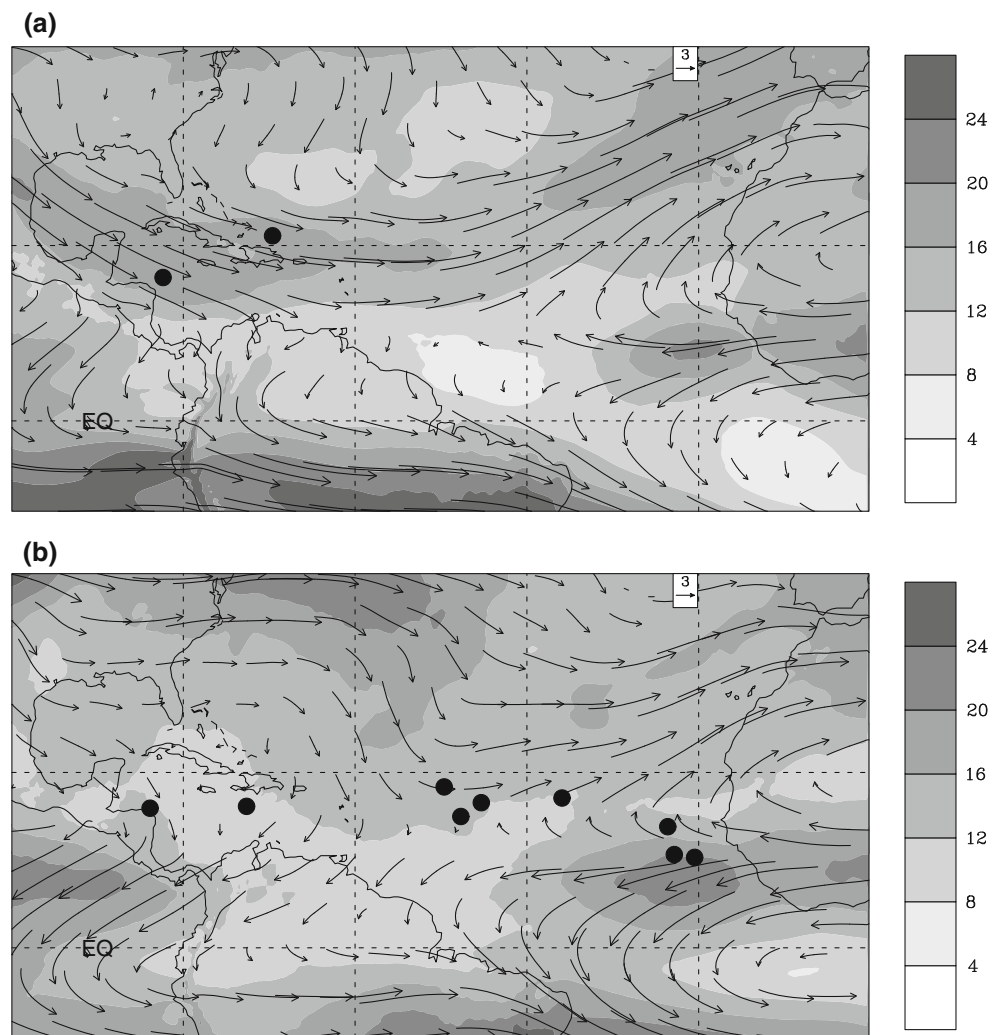
easterly shear and it is difficult to infer anything about the role of vertical wave accumulation for tropical cyclogenesis from this example analysis.

A quantitative analysis of the contribution of wave energy accumulation to tropical cyclone genesis compared with other environmental factors including shear, sea-surface temperature, mid-level moisture is the obvious next step and is the subject of future research as discussed in Sect. 6.

## 6 Conclusions

We have examined the role of wave energy accumulation in tropical cyclogenesis over the tropical North Atlantic. We adopted a hierarchical modeling approach starting with the simplified framework of the nonlinear shallow water equations. The experiments consisted of off-equatorial Rossby waves propagating through zonally varying background zonal flow scenarios that were representative of the lower atmospheric summer climate over the tropical North Atlantic. Regions of  $U_x < 0$  were shown to be wave

**Fig. 13** Vertical wind shear, defined as 200 hPa winds–850 hPa winds, (shaded,  $\text{m s}^{-1}$ ) and shear vectors for **a** June–July average and **b** August–September average. The 11 genesis locations of cyclones associated with easterly waves are marked by solid black circles



accumulation regions resulting in a reduction of the zonal wave scale, a decrease in both the flow relative and ground relative phase speeds and a substantial increase in local relative vorticity. Regions of  $U_x > 0$ , on the other hand, were shown to be regions of wave energy depletion. We find the relative contributions to changes in phase speed by divergence of advection by the mean flow and via scale contraction to be approximately equal. The theory of wave accumulation was also shown to be qualitatively correct for scenarios that did not satisfy scale separation outside the validity of the linear theory. This result has been shown previously (e.g. Farrell and Watterson 1985) but it is important to document here that the theory is also found to be robust for scenarios representative of the summer climate of the tropical North Atlantic.

The importance of wave accumulation for tropical cyclogenesis was then explored in a full physics and dynamics model. In a NRCM simulation of the tropical North Atlantic region for the entire 2005 hurricane season at 12 km grid spacing, 69% of easterly waves produced tropical cyclones in the months of August and September.

The 2-month mean dynamical environment showed regions of easterly winds increasing towards the east, consistent with the theory of wave accumulation. We hypothesize that the easterly waves within this period experienced modification through wave accumulation that contributed to cyclogenesis. The initial increase in ambient vorticity due to wave energy accumulation may have been sufficient to trigger convection-circulation feedbacks that can lead to cyclogenesis (as described in Sobel and Bretherton 1999). While there are clear limitations of assuming a 2-month mean field to be representative of the background flow at any one time within the 2-month period, we consider it to be adequate for our analysis. Genesis events for this study occurred in weak magnitude shear with no preference for the sign of the shear. Our investigation into the role of wave trapping in the vertical was therefore inconclusive.

Overall we have demonstrated the process of wave accumulation in a simple model setup designed to be representative of the summer climate of the tropical North Atlantic. Our analysis of a full physics and dynamics model simulation of the 2005 hurricane season is indicative of

wave accumulation contributing to cyclogenesis over the tropical North Atlantic and certainly indicates that wave accumulation should not be disregarded. Further research is underway to study wave accumulation in a controlled environment using an idealized version of the NRCM. This future work aims to quantify the contribution of wave energy accumulation to cyclogenesis relative to other environmental factors and deep moist convection.

Given the relative stability of the relevant features of the large-scale flow, this study indicates real potential to use waves as predictors in forecasting the probability of tropical cyclogenesis, perhaps drawing on the work by Wheeler and Weickmann (2001). This also may provide an explanation for the ability of global models to make useful predictions of cyclogenesis (e.g. Marin et al. 2009) and for the skill in seasonal forecasts of tropical storms (Vitart et al. 2007).

**Acknowledgments** We thank Hai-Ru Chang for help with the appendix and we thank the Geophysical Fluid Dynamics Laboratory's Flexible Modeling System for providing the shallow water model code. NCAR is sponsored by the National Science Foundation and this work was supported by the Willis Research Network. This manuscript was improved through comments by two anonymous reviewers.

## Appendix

Consider the shallow water equations on an equatorial  $\beta$ -plane with an equivalent depth  $h$ . Solutions for the horizontal components of velocity are:

$$v_n = Ae^{-\frac{z^2}{2}} H_n(\xi) e^{i(kx + \omega_n t)} \quad (12)$$

$$u_n = -iAc \sqrt{\frac{\beta}{c}} e^{-\frac{z^2}{2}} \left[ \frac{n H_{n-1}(\xi)}{\omega_n - kc} + \frac{1 H_{n+1}(\xi)}{2\omega_n + kc} \right] e^{i(kx + \omega_n t)} \quad (13)$$

where  $c = \sqrt{gh}$ ,  $k$  and  $n$  correspond to the zonal and meridional wave numbers respectively, the non-dimensional meridional coordinate  $\xi = \sqrt{\beta/cy}$  and the angular frequency  $\omega_n$  is defined as:

$$\omega_n = -\bar{U}k + \frac{\beta k}{k^2 + \frac{\beta}{c}(2n+1)} \quad (14)$$

In  $\xi$ -space, the Hermite polynomials ( $H_n(\xi)$ ) are defined as:

$$H_0(\xi) = 1 \quad (15)$$

$$H_1(\xi) = 2\xi \quad (16)$$

$$H_2(\xi) = 4\xi^2 - 2 \quad (17)$$

$$H_3(\xi) = 8\xi^3 - 12\xi \quad (18)$$

$$H_4(\xi) = 16\xi^4 - 48\xi^2 + 12 \quad (19)$$

We note that the relative vorticity for the  $n$ th mode is given by:

$$\zeta_n = \frac{\partial v_n}{\partial x} - \frac{\partial u_n}{\partial y} \quad (20)$$

Consider solutions for  $n = 1$ : (12) and (15) give:  $v_1 = Ae^{-\frac{z^2}{2}} 2\xi e^{i(kx + \omega_1 t)}$  and (13), (14) and (16) give:  $u_1 = -iA\sqrt{c\beta} e^{-\frac{z^2}{2}} \left[ \frac{1}{\omega_1 - kc} + \frac{2\xi^2 - 1}{\omega_1 + kc} \right] e^{i(kx + \omega_1 t)}$  so that, after some manipulation:

$$\zeta_1 = iA e^{-\frac{z^2}{2}} e^{i(kx + \omega_1 t)} \left[ 2k\xi - \beta \left( \frac{\xi}{\omega_1 - kc} + \frac{2\xi^3 - 5\xi}{\omega_1 + kc} \right) \right] \quad (21)$$

Consider solutions for  $n = 2$ : After (much) manipulation one finds (identically as to 21):

$$\zeta_2 = iA e^{-\frac{z^2}{2}} e^{i(kx + \omega_2 t)} \times \left[ k(4\xi^2 - 2) - \beta \left( \frac{4\xi - 4}{\omega^2 - kc} + \frac{4\xi^3 - 18\xi + 6}{\omega^2 + kc} \right) \right] \quad (22)$$

and so on for higher  $n$ . Now, relative vorticity is not conserved but we know from conservational principles that along a ray where  $d\bar{U}/dx \neq 0$  that:

$$\frac{dk}{dt} = -k \frac{d\bar{U}}{dx} \quad (23)$$

Thus, if we can calculate the change of  $k$  in a stretching deformation field, then we can calculate the relative vorticity.

## References

- Barrett BS, Leslie LM (2009) Links between tropical cyclone activity and Madden-Julian Oscillation phase in the North Atlantic and northeast Pacific basins. *Mon Weather Rev* 137:727–744
- Bretherton FP, Garrett CJR (1968) Wavetrain in inhomogeneous moving media. *Proc R Soc Lond A* 362:529–554
- Briegleb LM, Frank WM (1997) Large-scale influences on tropical cyclogenesis in the western North Pacific. *Mon Weather Rev* 125:1397–1413
- Chang H-R, Webster PJ (1990) Energy and accumulation and emanation at low latitudes. Part II: nonlinear response to strong episodic equatorial forcing. *J Atmos Sci* 47:2624–2644
- Davis C, Wang W, Chen SS, Chen Y, Corbosiero K, DeMaria M, Dudhia J, Holland G, Klemp J, Michalakes J, Reeves H, Rotunno R, Snyder C, Xiao Q (2008) Prediction of landfalling hurricanes with the advanced hurricane WRF model. *Mon Weather Rev* 136:1990–2005
- Done JM, Leung LR, Kuo Y-H (2006) Understanding error in the long-term simulation of warm season rainfall using the WRF model. In: 7th WRF users workshop, Boulder, CO, USA (Extended Abstract)
- Farrell W, Watterson I (1985) Rossby waves in opposing currents. *J Atmos Sci* 42:1746–1756
- Frank WM, Clark GB (1980) Atlantic tropical systems of 1979. *Mon Weather Rev* 108:966–972

- Frank WM, Roundy PE (2006) The role of tropical waves in tropical cyclogenesis. *Mon Weather Rev* 134:2397–2417
- Gill AE (1980) Some simple solutions for heat-induced tropical circulation. *Q J Roy Met Soc* 106:447–462
- Giorgi F, Marinucci M, Bates G (1993) Development of a second-generation regional climate model RegCM2. Part II: convective processes and assimilation of lateral boundary conditions. *J Clim* 121:2814–2832
- Gray WM (1968) Global view of the origin of tropical disturbances and storms. *Mon Weather Rev* 96:669–700
- Holland GJ (1995) Scale interaction in the western Pacific monsoon. *Meteor Atmos Phys* 56:57–79
- Holland GJ, Done J, Bruyere C, Cooper C, Suzuki-Parker A, (2010) Model investigations of the effects of climate variability and change on future Gulf of Mexico tropical cyclone activity. OTC 20690. [http://www.mmm.ucar.edu/people/holland/files/OTC2010\\_Future\\_Hurricanes\\_Submitted.pdf](http://www.mmm.ucar.edu/people/holland/files/OTC2010_Future_Hurricanes_Submitted.pdf)
- Hsieh J-S, Cook KH (2005) Generation of African easterly wave disturbances: relationship to the African easterly jet. *Mon Weather Rev* 133:1311–1327
- Kieu CQ, Zhang D-L (2008) Genesis of Tropical Storm Eugene (2005) from merging vortices associated with the ITCZ breakdowns. Part I: observational and modeling analyses. *J Atmos Sci* 65:3419–3439
- Kuo H-C, Chen J-H, Williams RT, Chang C-P (2001) Rossby waves in zonally opposing mean flow: behavior in northwest Pacific summer monsoon. *J Atmos Sci* 58:1035–1050
- Landsea CW (1993) A climatology of intense (or major) Atlantic hurricanes. *Mon Weather Rev* 121:1703–1713
- Li T, Fu B, Ge X, Wang B, Peng M (2003) Satellite data analysis and numerical simulation of tropical cyclone formation. *Geophys Res Lett* 30:2122. doi:10.1029/2003GL018556
- Liang X-Z, Kunkel K, Samel A (2001) Development of a regional climate model for U.S. Midwest applications. Part I: sensitivity to buffer zone treatment. *J Clim* 14:4363–4378
- Lighthill J (1978) *Waves in fluids*. Cambridge University Press, Cambridge, p 504
- Maloney ED, Hartmann DL (2000) Modulation of hurricane activity in the Gulf of Mexico by the Madden-Julian oscillation. *Science* 287:2002–2004
- Marin JC, Raymond DJ, Raga GB (2009) Intensification of tropical cyclones in the GFS model. *Atmos Chem Phys* 9:1407–1417
- Molinari J, Lombardo K, Vollaro D (2007) Tropical cyclogenesis within an equatorial Rossby wave packet. *J Atmos Sci* 64:1301–1317
- Pasch RJ, Avila LA, Jiing JG (1998) Atlantic tropical systems of 1994 and 1995: a comparison of a quiet season to a near-record-breaking one. *Mon Weather Rev* 126:1106–1123
- Reed RJ, Hollingsworth A, Heckley WA, Delsol F (1988) An evaluation of the performance of the ECMWF operational system in analyzing and forecasting easterly wave disturbances over Africa and the tropical Atlantic. *Mon Weather Rev* 116:824–865
- Ritchie EA, Holland GJ (1999) Large-scale patterns associated with tropical cyclogenesis in the western Pacific. *Mon Weather Rev* 127:2027–2043
- Skamarock WC, Klemp JB, Dudhia J, Gill DO, Barker DM, Wang W, Powers JG (2005) A description of the advanced research WRF Version 2. NCAR Technical Note TN-468+STR, 88pp
- Sobel AH, Bretherton CS (1999) Development of synoptic-scale disturbances over the summertime tropical northwest Pacific. *J Atmos Sci* 56:3106–3127
- Swanson KL (2008) False causality between Atlantic hurricane activity fluctuations and seasonal lower atmospheric wind anomalies. *Geophys Res Lett* 35:L18807. doi:10.1029/2008GL034469
- Tam C-Y, Li T (2006) The origin and dispersion characteristics of the observed tropical summertime synoptic-scale waves over the western Pacific. *Mon Weather Rev* 134:1630–1646
- Thorncroft C, Hodges K (2001) African easterly wave variability and its relationship to Atlantic tropical cyclone activity. *J Clim* 14:1166–1179
- Tulich SN, Kiladis GN, Suzuki-Parker A (2009) Convectively coupled Kelvin and easterly waves in a regional climate simulation of the tropics. *Clim Dyn*. doi:10.1007/s00382-009-0697-2
- Vitart F, Huddleston MR, Déqué M, Peake D, Palmer TN, Stockdale TN, Davey MK, Ineson S, Weisheimer A (2007) Dynamically based seasonal forecasts of Atlantic tropical storm activity issued in June by EUROSIP. *Geophys Res Lett* 34:L16815. doi:10.1029/2007GL030740
- Webster PJ (1972) Response of the tropical atmosphere to local steady forcing. *Mon Weather Rev* 100:518–541
- Webster PJ, Chang H-R (1988) Equatorial energy accumulation and emanation regions: impacts of a zonally varying basic state. *J Atmos Sci* 45:803–829
- Webster PJ, Chang H-R (1997) Atmospheric wave propagation in heterogeneous flow: basic flow controls on tropical-extratropical wave modification. *Dyn Atmos Oceans* 27:91–134
- Wheeler M, Kiladis GN (1999) Convectively coupled equatorial waves: analysis of clouds and temperature in the wavenumber-frequency domain. *J Atmos Sci* 56:374–399
- Wheeler M, Weickmann K (2001) Real time monitoring of modes of coherent synoptic to intraseasonal convective variability. *Mon Weather Rev* 129:2677–2694
- Wheeler M, Kiladis GN, Webster PJ (2000) Large-scale dynamical fields associated with convectively coupled equatorial waves. *J Atmos Sci* 57:613–640
- Whitham GB (1965) A general approach to linear and non-linear dispersive waves using a Lagrangian. *J Fluid Mech* 22:273–283